Dalton Transactions

Accepted Manuscript

ROYAL SOCIETY OF CHEMISTRY

www.rsc.org/dalton

Solvent assisted formation of ruthenium(III) and ruthenium(II) hydrazone complexes in one-pot with potential *in vitro* cytotoxicity and enhanced LDH, NO and ROS release

Eswaran Jayanthi,[a] Sivalingam Kalaiselvi,[b] Viswanatha Vijaya Padma, [b] Nattamai S.P.Bhuvanesh,[c] Nallasamy Dharmaraj [a]

[a]Inorganic & Nanomaterials Research Laboratory, Department of Chemistry, Bharathiar University, Coimbatore – 641 046, India. E-mail: dharmaraj@buc.edu.in;

Tel.: +91 422 2428319; Fax: +91 422 2422387.

[b]Department of Biotechnology, Bharathiar University, Coimbatore 641 046, India.

[c]Department of Chemistry, Texas A&M University, College Station, TX 77843, U.S.A.

Abstract

A set each of new bivalent and trivalent ruthenium complexes, $[Ru^{III}(HL)Cl_2(EPh_3)_2]$ and $[Ru^{II}(L)(CO)\ (EPh_3)_2]$ (E= P (complexes **1** and **2**) or As (complexes **3** and **4**)) were synthesised from the reactions of $[Ru^{III}Cl_3(EPh_3)_3]$ with 2-hydroxynaphthaldehyde benzoic acid hydrazone (**H_2L**) in methanol-chloroform and characterized by elemental analysis, spectral data and XRD study. A suitable mechanism to account for the formation of bivalent ruthenium carbonyl complexes from the corresponding trivalent precursors is provided by considering the role of added base in the reaction. Interaction of complexes **1-4** with CT-DNA/BSA was analysed with absorption and emission spectral titration studies. *In vitro* cytotoxic potential of the above ruthenium hydrazone complexes **1-4** assayed against A549 cell line revealed a significant growth inhibition. The test complexes **1-4** added in IC_{50} concentration into the cell culture medium enhanced the release of LDH, NO and ROS in comparison with control. Cell death induced by the complexes studied using propidium iodide (PI) staining assay exhibited noticeable changes in the cell morphology resembling that of an apoptosis.

Introduction

Cancer, one of the most deadly diseases in the world causes severe health problems and led to millions of death among affected every year. As a result, exploration of anticancer drugs has become an imperative field in pharmaceutical research. Platinum based anticancer drugs gained an extensive attention of researchers and marked a new epoch in cancer therapy. They could covalently bind with purines of DNA and thus induce distortion in DNA and prohibit cancer cell replication and its growth. Though 70% of all cancer patients receive platinum based drugs during treatment, a key problem with these drugs is the so called "off-target" effects wherein non-cancerous cells are affected by DNA modification reactions that leads to drug induced toxicity, side effects and little margin for error between the therapeutic dose and the toxic dose.[1,2] Recently, ruthenium complexes with excellent cytotoxic potential with low levels of side effects draw attention as second generation metal based anticancer drugs. Two new ruthenium complexes [HIm]-*trans*-[$RuCl_4$(DMSO)(Im)] (NAMI-A) and [HInd]*trans*-[$RuCl_4(Ind)_2$] (KP1019) after successful completion of extensive preclinical and phase I clinical trials currently entered into further clinical investigations. In spite of their meek cytotoxic activity, these complexes have attracted significant interest because of their ability to prevent the formation of metastases and inhibit their growth.[3, 4] DNA is one of the major putative targets for all these metal based anticancer drugs. Generally, these drugs coordinate/intercalate with DNA, aid in the damage of DNA and in turn enhance their cytotoxic effect.[5,6] In addition to DNA, considerable attention has been focused on the interaction of drugs with proteins by researchers owing to their functions in transportation of several endo- and exogenous compounds.[7] Of the many plasma proteins those interact with drugs, albumins are the most important multifunctional transport protein due to their ability to bind reversibly to a variety of ligands and exert an important effect on the distribution and metabolism of the drug in the blood stream. Albumin binding can escalate the solubility of the drugs and thus extend its *in vivo* half-life that enhances the bioavailability of a drug.[8] Serum albumin interaction is thus considered as a key factor in the *in vivo* activity of drugs.[9] For ruthenium-based agents, albumin acts as a Ru-compound store house.[10] Apart from that, ruthenium complexes are found to raise the level of intracellular ROS and thus damage the cancer cells through mitochondrial mediated pathway.[11]

Nitrogen containing compounds are active occupants of biomolecules and play vital role in the biological system. Hydrazones are nitrogen containing compounds with varied biological activities.[12] It is well established that the formation of metal complexes with

hydrazones play an important role to enhance the biological properties and biomolecular interactions than that of free hydrazones.[13] In spite of several reports on the synthesis and biological evaluation of ruthenium complexes of various hydrazone ligand systems,[14] similar work on 2-hydroxynaphthaldehyde benzoic acid hydrazone (H_2L) remains unexplored. In continuation of our journey on the synthesis and pharmacological evaluation of various transition metal hydrazone complexes, in the present case, the said hydrazone was chosen as a ligand to synthesize new ruthenium complexes $[Ru^{III}(HL)Cl_2(PPh_3)_2]$(**1**), $[Ru^{II}(L)(CO)(PPh_3)_2]$(**2**), ($[Ru^{III}(HL)Cl_2(AsPh_3)_2]$(**3**) and $[Ru^{II}(L)(CO)(AsPh_3)_2]$(**4**) and to probe the role of oxidation state of metal ion and co-ligands in effecting DNA /protein binding, *in vitro* cytotoxicity through apoptosis of such complexes towards A549 cell line.

Experimental

General

All the chemicals used for the preparation of ligand, complexes and buffers are of analytically or chemically pure grade and were used without further purification. $RuCl_3{\cdot}3H_2O$ was purchased from Hi-Media. The starting complexes, $[RuCl_3(PPh_3)_3]$[15], $[RuCl_3(AsPh_3)_3]$ [16] and the ligand, 2-hydroxynaphthaldehyde benzoic acid hydrazone (**H_2L**)[17] were prepared according to reported methods. Doubly distilled water was used to prepare buffers. Protein free calf thymus DNA (CT-DNA), obtained from Sigma-Aldrich chemicals was stored at 0–4 °C and its purity was checked by measuring its optical density before use. Doubly distilled water was used to prepare Tris–HCl buffer (5 mM Tris–HCl, 50 mM NaCl, pH 7.2, Tris–Tris(hydroxymethyl)methylamine). DNA stock solutions were freshly prepared before study using this buffer solution. Ethidium bromide and 3-(4, 5-dimethylthiazol-2-yl)-2,5-diphenyltetrazoliumbromide (MTT) were purchased from Sigma-Aldrich and used as received. Elemental analysis (C, H and N) of the powdered samples were performed on a Vario EL III Elemental analyser. IR spectra of the compounds were recorded as KBr pellets with a Nicolet Avatar Model FT-IR spectrophotometer in the range 4000–400 cm^{-1}. Melting points of the complexes were determined with a Lab India instrument. Electronic absorption spectra of the samples were recorded using a Jasco V-630 spectrophotometer. Emission spectra were measured using a Jasco FP 6600 spectrofluorometer. Mass spectra of the complexes **1**-**4** were taken using LCQ Fleet, Thermo Fisher Mass spectrometer. EPR spectra were recorded on JES-X3 SERIES EPR spectrometer at X-band frequencies for powdered samples at 278 K with microwave power 0.99800 [mW], modulation amplitude 25 and the

field being calibrated with 2,2-diphenyl-1-picrylhydrazyl radical (DPPH, g = 2.0037). ^{1}H NMR spectra were recorded on a Bruker Avance-3 spectrometer at 400 MHz. Non-small cell lung cancer cell line (A549) was obtained from the National Centre for Cell Science (NCCS), Pune, India. All other chemicals and reagents used for the biological studies were of high quality and procured commercially from reputed suppliers.

One-pot synthesis of new ruthenium–hydrazone complexes

Synthesis of $[Ru^{III}(HL)Cl_2(PPh_3)_2]$(1) and $[Ru^{II}(L)(CO)(PPh_3)_2]$(2): A solution of $[RuCl_3(PPh_3)_3]$ (0.2485 g; 0.25 mM) in 10 mL of chloroform was refluxed with equimolar quantity of the ligand H_2L (0. 0582 g; 0.25 mM) in 10 mL of methanol for 10 h (scheme 1). During the course of the reaction, a brown colour product precipitated out from the reaction mixture was filtered and recrystallized from 1:1 ratio of MeOH/$CHCl_3$ mixture to get blocks of complex **1** suitable for single-crystal X-ray diffraction studies and formulated as $[Ru^{III}(HL)Cl_2(PPh_3)_2]$(**1**). The filtrate monitored by TLC revealed the presence of an another product that was isolated upon slow evaporation as plate like orange crystals identified as $[Ru^{II}(L)(CO)(PPh_3)_2]$(**2**).

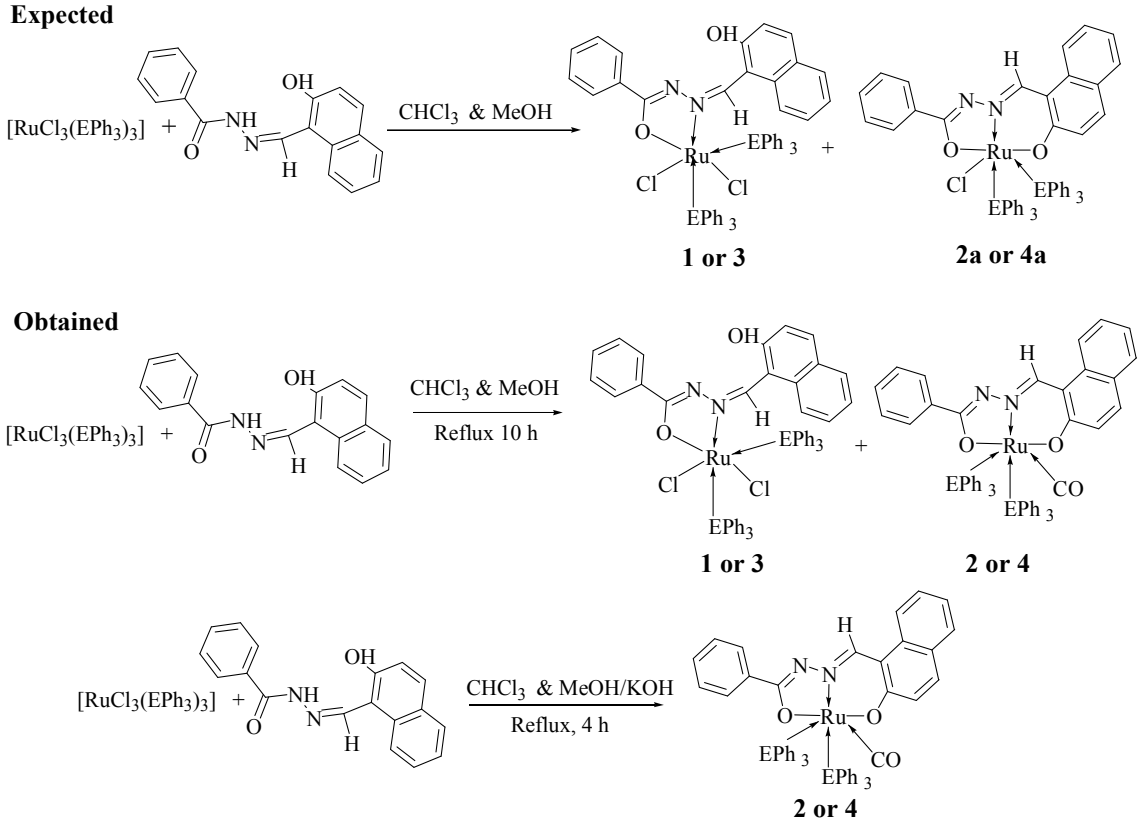

Scheme 1. Synthesis of ruthenium hydrazone complexes **1 - 4.**

$[Ru^{III}(HL)Cl_2(PPh_3)_2]$(1). Yield: 53% (0.1248 g, 0.132 mm). Colour: Brown; Melting point: >206 °C. Elemental analysis Found (calcd) (%) for $C_{54}H_{43}Cl_2N_2O_2P_2Ru$ (%): C, 65.62 (65.79); H, 4.33 (4.39); N, 2.81 (2.84). UV−vis (5% DMSO in buffer), λ_{max} (nm), ε (M^{-1} cm^{-1}):275 (20331), 390 (4328), 444 (3141), 472 (3319). IR (KBr disks, cm^{-1}): 1571,1508 (s) ν(C=N); 1329 ν(enolic, C–O); 1092 ν(N–N); 1431, 1092, 694 (for PPh_3). ESI-MS: calcd. For $C_{54}H_{43}Cl_2N_2O_2P_2Ru$ is 985.85; found $[M + H]^+$: 986.96.

$[Ru^{II}(L)(CO)(PPh_3)_2]$(2). Yield: 12 % (0.0296 g, 0.030 mm). Colour: orange; Melting point: >200 **°C**. Elemental analysis Found (calcd) (%) for $C_{55}H_{42}N_2O_3P_2Ru$ (%): C, 70.06(70.13); H, 4.45 (4.49); N, 2.91 (2.97). UV−vis (5% DMSO in buffer), λ_{max} (nm), ε (M^{-1} cm^{-1}): 266(40836), 332 (15299), 384 (15818), 436 (8620).IR (KBr disks, cm^{-1}): 1583, 1509 (s) ν (C=N); 1353 ν(enolic, C–O); 1078 ν(N–N); 1945 ν(Ru-CO); 1433, 1078, 693 (for PPh_3).^{1}H NMR($CDCl_3$): δ 8.84(s, 1H, HC═N); 7.81-6.80(m,41 H, Ar-H). ESI-MS: calcd. For $C_{55}H_{42}N_2O_3P_2Ru$ is 941.95; found $[M + H]^+$: 943.02.

Synthesis of complexes $[Ru^{III}(HL)Cl_2(AsPh_3)_2]$(3) and $[Ru^{II}(L)(CO)(AsPh_3)_2]$(4)

Complexes **3** & **4** were prepared by a procedure similar to that used for complexes **1** & **2** by reacting equimolar quantity of the ligand (H_2L)(0.0582 g; 0.25 mM) in 10 mL of methanol and $[RuCl_3(AsPh_3)_3]$ (0. 282 g; 0.25 mM) in 10 mL of chloroform (Scheme 1).

$[Ru^{III}(HL)Cl_2(AsPh_3)_2]$(3). (Yield: 49% (0.1315 g, 0.123 mm). Colour: Brown; Melting point: >154°C. Elemental analysis Found (calcd) (%) for $C_{54}H_{43}Cl_2N_2O_2As_2Ru$ (%): C, 60.32 (60.40); H, 3.98 (4.04); N, 2.54 (2.61). UV−vis (5% DMSO in buffer), λ_{max} (nm), ε (M^{-1} cm^{-1}): 263(43860), 329(19129), 376(14037), 429 (10830). IR (KBr disks, cm^{-1}): 1595,1509 (s) ν(C=N–N=C); 1351 ν(enolic, C–O); 1073 ν(N–N); 1435, 1078, 692 (for $AsPh_3$). ESI-MS: calcd. For $C_{54}H_{43}Cl_2N_2O_2As_2Ru$ is 1073.75; found $[M + H]^+$: 1074.85.

$[Ru^{II}(L)(CO)(AsPh_3)_2]$ (4). Yield: 10% (0.02575 g, 0.025 mm). Colour: Brown; Melting point: >152 °C. Elemental analysis Found (calcd) (%) for $C_{55}H_{42}N_2O_3As_2Ru$ (%): C, 64.09 (64.14); H, 4.02 (4.11); N, 2.63 (2.72). UV−vis (5% DMSO in buffer), λ_{max} (nm), ε (M^{-1} cm^{-1}): 263(34441), 329 (13632), 381 (10347). IR (KBr disks, cm^{-1}): 1583,1508 ν(C=N); 1351 ν(enolic C–O); 1077 ν(N–N); 1945 ν(Ru-CO); 1432, 1077, 694 (for $AsPh_3$).^{1}H

NMR($CDCl_3$): δ 8.74(s, 1H, HC═N); 7.38-7.16 (m,41 H, Ar-H). ESI-MS: calcd. For $C_{55}H_{42}N_2O_3As_2Ru$ is 1029.85; found $[M + H]^-$: 1030.85.

Synthesis of complexes $[Ru^{II}(L)(CO)(PPh_3)_2]$(2) or $[Ru^{II}(L)(CO)(AsPh_3)_2]$(4) in presence of a base

A solution of $[RuCl_3(EPh_3)_3]$ (where E=P or As) (0.2485 g; 0.25 mM)/(0. 2820 g; 0.25 mM) in 10 mL of chloroform was refluxed with equimolar quantity of the ligand H_2L (0. 0582 g; 0.25 mM) in presence of KOH (0.0281g; 0.5 mM) in 10 mL of methanol for 4 h (Scheme 1) to obtain the complex $[Ru^{II}(L)(CO)(PPh_3)_2]$**(2)** or $[Ru^{II}(L)(CO)(AsPh_3)_2]$**(4)** as sole products from the respective reactions.

$[Ru^{II}(L)(CO)(PPh_3)_2]$(2). Yield: 47%

$[Ru^{II}(L)(CO)(AsPh_3)_2]$(4). Yield: 43%

Single crystal X-ray diffraction studies. The single crystal X-ray diffraction data of complexes **1, 2** and **4** were collected on a BRUKER GADDS X-ray (three-circle) diffractometer and the goniometer was controlled using the FRAMBO software, v.4.1.05, but for complex **3** using BRUKER APEX 2 X-ray (three-circle) diffractometer and the goniometer was controlled using the APEX2 software suite, v2008-6.0.by using MoKα (λ= 0.70173 Å).The integrated intensity information for each reflection was obtained by a reduction of the data frames with the program APEX2.[18] Single crystal data collections and corrections for the new Ru complexes (**1, 2** and **4**) were done at 110 K using graphite monochromated Cu Kα (λ = 1.5418 Å) radiation and the integration method employed a three dimensional profiling algorithm and all of the data were corrected for Lorentz and polarization factors, as well as for crystal decay effects. Finally the data were merged and scaled to produce a suitable data set. A solution was obtained readily using SHELXTL (SHELXS and XS).[19] The solvent molecules in complex **1** could not be identified because of significant disorder and partial occupancy and hence they were squeezed out using PLATON.[20] Accordingly, the density and the formula reported in the CIF file and the table does not account for the solvation in case of complex **1**. In all other complexes (**2-4**), the solvent molecules were identified and included in CIF file. The hydrogen atoms were placed in idealized positions and were set riding on the respective parent atoms. In complexes **2** and **4**, the phenyl group (C13 - C18) was found disordered between two positions with a ratio of 0.46:0.54 and 0.53:0.47 respectively and was modelled successfully. All non-hydrogen atoms

were refined with anisotropic thermal parameters. The structure was refined (weighted least squares refinement on F2) to convergence.[19, 21]

DNA interaction studies by electronic absorption experiments. Interaction of ruthenium hydrazone complexes **1-4** with CT-DNA was studied using UV-visible spectroscopy in order to explore the possible binding modes of them with CT-DNA and to calculate the binding constants. CT-DNA stock solutions were prepared using Tris-HCl buffer (5 mmol, pH-7.2), kept at 4° C and utilised for a maximum of 4 days. A solution of CT-DNA in the buffer gave a ratio of UV absorbance of about 1.8-1.9 at 260 and 280 nm, indicating that the DNA was sufficiently free of protein.[22] The concentration of CT-DNA was obtained from its absorption spectrum using the molar extinction coefficient value of 6600 M^{-1} cm^{-1} at 260 nm. The complexes dissolved in DMSO and Tris–HCl (5:95) was used in all the experiments. Absorption titration experiments were performed with a fixed concentration of the compounds while gradually increasing the concentration of DNA. The blank Tris-HCl buffer solution and the ruthenium complexes were placed in reference and test cuvettes respectively. To eliminate the absorbance of DNA, an equal amount of DNA was added to both the cuvettes. The extent of the binding of the complexes **1-4** with CT-DNA was identified from the binding constant K_b, that was obtained by monitoring the changes in the absorbance of the corresponding λ_{max} with increasing concentrations of CT-DNA and is given by the equation

$$[DNA]/[\varepsilon_a-\varepsilon_f] = [DNA]/[\varepsilon_b-\varepsilon_f] + 1/K_b[\varepsilon_b-\varepsilon_f] \quad (1)$$

Where [DNA] is the concentration of DNA in the base pairs, ε_f is the extinction coefficient of the complex in free solution and $\varepsilon_b$is the extinction coefficient of the complex when fully bound to DNA. A plot of $[DNA]/[\varepsilon_b-\varepsilon_f]$ versus [DNA] gave a slope and the intercept equal to $1/[\varepsilon_a-\varepsilon_f]$ and $(1/K_b)[\varepsilon_b-\varepsilon_f]$, respectively. The intrinsic binding constant K_b is calculated from the ratio of the slope to the intercept.

Fluorescence quenching experiments. Competitive binding experiments of DNA with EB were carried out in Tris buffer by keeping [DNA]/[EB] constant and varying the concentrations of the ruthenium complexes in order to analyse whether the complex displaces EB from its DNA–EB complex. The fluorescence spectra of EB bound DNA was obtained in the excitation and the emission wavelengths of 515 and 602 nm, respectively. Before measurements, the system was shaken and incubated at room temperature for 5 min. The

emission was recorded at 530–750 nm. The quenching constants of complexes **1-4** were evaluated qualitatively by employing Stern–Volmer equation,[23]

$$I_0/I = K_q [Q] + 1 \qquad (2)$$

where, I_0 and I are the emission intensities in the absence and in the presence of quencher, K_q is the quenching constant, [Q] is the quencher concentration. K_q is the slope, obtained from the plot of I_0/I vs [Q]. The apparent binding constant (K_{app}) values were obtained for the compounds using the following equation,[24]

$$K_{EB} [EB] = K_{app} [compound] \qquad (3)$$

$K_{EB}=1.0\times10^7\ M^{-1}$ and [EB] = 10 μM.

Protein binding studies. The binding of ruthenium complexes with BSA was assessed by tryptophan fluorescence quenching experiments conducted with increasing concentration of complexes as quenchers, at the excitation and emission wavelengths of BSA at 280 nm and 345 nm respectively. The excitation and emission slit widths and scan rates were maintained uniform for all the experiments. Stock solution of BSA was made in 50 mM phosphate buffer (pH, 7.4) and stored in the dark at 4 °C for further use. Concentrated stock solutions of the complexes were prepared by dissolving them in DMSO: phosphate buffer (5:95) and diluted suitably with phosphate buffer to required concentrations. Synchronous fluorescence spectra were also recorded simultaneously using the same concentration of BSA and complexes with two different Δλ value such as 15 and 60 nm (difference between the excitation and emission wavelengths of BSA) at which the spectrum only shows the spectroscopic acquit of the tyrosine and tryptophan residues of the BSA protein respectively. To study the interactions of quencher with serum albumin, the Stern-Volmer and Scatchard plots were used. The fluorescence quenching data were analysed with the Stern–Volmer quenching equation,[25]

$$I_0/I = 1 + K_q\tau_0[Q] \quad = 1 + K_{SV} \qquad (4)$$

Where I_0= the initial tryptophan fluorescence intensity of SA, I = the tryptophan fluorescence intensity of SA after the addition of the quencher, K_q = the quenching rate constant of SA, K_{SV} =the dynamic quenching constant, τ_0 = the average lifetime of SA without the quencher and [Q] = the concentration of the quencher. The K_{SV} value obtained as slope from the plot of I_0/I versus [Q].

When small molecules bind independently to a set of equivalent sites on a macromolecule, the equilibrium between free and bound molecules is represented by the Scatchard equation,[25]

$$\log [F_0\text{-}F/F] = \log K_{bin} + n \log [Q] \qquad (5)$$

where, K_{bin} and n are the binding constant and the number of binding sites, respectively. Thus, a plot of log $[F_0\text{-}F/F]$ versus log [Q] can be used to determine the values of both the binding constant (K_{bin}) and number of binding sites n.

In vitro evaluation of anticancer activity.

Cell viability. Using 3-(4, 5-dimethylthiazol-2-yl)-2, 5-diphenyltetrazolium bromide (MTT), effect of complexes **1-4** on the viability of A549 cells was assayed.[26] The cells were seeded at a density of 10,000 cells per well, in 200 mL Dulbecco's Modified Eagle's Medium (DMEM) and were allowed to attach overnight in a CO_2 incubator. Then media were flicked off and the complexes dissolved in DMSO and diluted in cell culture media were added to the cells at a final concentration of 1, 5, 10 and 25 μM. After 48 h, the wells were treated with 20 mL MTT (5 mg/mL PBS (Phosphate buffered saline)) and incubated at 37 °C for 4 h. The purple formazan crystals formed were dissolved in 200 mL DMSO and read at 570 nm in a micro plate reader. All measurements were made in triplicate and the medium containing no test compound served as the control. The % cell inhibition was determined using the following formula and the graph was plotted of % cell inhibition versus concentration. The IC_{50} values were calculated from the graph by means of the equation:

$$\% \text{ Cell inhibition} = [100 - \text{Abs}_{(drug)} / \text{Abs}_{(control)}] \times 100. \qquad (6)$$

Release of lactate dehydrogenase. LDH activity was determined by the linear region of a pyruvate standard graph using regression analysis and expressed as percentage (%) leakage as described previously.[27] Briefly, to a set of tubes, 1 mL of buffered substrate (lithium lactate) and 0.1 mL of the medium were added and tubes were incubated at 37 °C for 30 min. After adding 0.2 mL of nicotinamide adenine dinucleotide (NAD) solution, the incubation was continued for another 30 min. The reaction was then arrested by adding 0.1 mL of dinitrophenylhydrazine (DNPH**)** reagent and the tubes were incubated for further period of 15 min at 37°C. After this, 0.1 mL of medium was added to blank tubes after arresting the

reaction with DNPH. 3.5 mL of 0.4 N sodium hydroxide was added to all the tubes. The colour developed was measured at 420 nm in a Shimadzu UV/visible spectrophotometer. The amount of LDH released was expressed as percentage.

Nitric oxide (NO) assay. The amount of nitrite was determined by using Griess reaction assay.[28] To 100 µL of the medium, 50 mL of Griess reagent-I was added, mixed and allowed to react for 10 min. This was followed by the addition of 50 µL of Griess reagent-II and the reaction mixture was mixed well and incubated for another 10 min at room temperature. The pink colour developed was measured at 540 nm in a microquant plate reader (Biotek Instruments).

Measurement of intracellular ROS generation. 2', 7' -Dichlorodihydrofluorescein diacetate (DCF-DA) was used to evaluate the intracellular ROS level in the form of cellular peroxides. This cell-permeant dye is hydrolysed by intracellular esterases into its nonfluorescent form (DCFH) and then it is oxidized by intracellular free radicals to produce a fluorescent product, namely dichlorofluorescein (DCF). In a typical assay, cells were seeded at a density of 1×10^5 cells/well and were incubated with 25 mL of DCF-DA (5 mg/mL) for 30 min, followed by incubation with IC_{50} concentration of complexes (**1-4**) for different time periods (15, 30 and 60 min). Then, they were centrifuged, washed and resuspended in PBS and read in a Jasco FP 6600 spectrofluorometer with an excitation at 480 nm and corresponding emission at 520 nm. The values were expressed as % DCF fluorescence as compared to the control.[29]

Apoptotic cell detection by propidium iodide. A549 cells were treated with IC_{50} concentration of complexes **1- 4** for 48 h, collected, washed with PBS, fixed overnight with 70% ethanol at 4 °C and incubated with PI at room temperature for 30 min and nuclear morphology was examined using fluorescence microscope.

Results and discussion

Synthesis and characterization. A pair each of new ruthenium(III) complexes ([$Ru^{III}(HL)(Cl_2)(PPh_3)_2$](**1**) and [$Ru^{III}(HL)Cl_2(AsPh_3)_2$](**3**)) and ruthenium(II) complexes ([$Ru^{II}(L)(CO)(PPh_3)_2$](**2**) and [$Ru^{II}(L)(CO)(AsPh_3)_2$](**4**)) respectively containing hydrazone as a primary ligand and PPh_3/$AsPh_3$ as co-ligands were synthesized from the reactions of precursors [$RuCl_3(PPh_3)_3$] or [$RuCl_3(AsPh_3)_3$] and the hydrazone ligand **(H_2L)** as specified in Scheme 1. Though the formation of trivalent ruthenium complexes **2a** and **4a** is well expected from these reactions, complexes **1** and **3** are also quite possible based on the

coordination diversity point of view of the ligand **H_2L**. But, we were surprised to get new bivalent ruthenium complexes **2** and **4** as minor products in addition to **1** and **3** without any trace of **2a** and **4a**. Upon knowing the crystal structure of complexes **1** and **3** wherein the hydrazone ligand possesses the free phenolic –OH even after coordination through other sites to ruthenium ion propelled us to investigate the same reaction by adding a strong base like KOH that could deprotonate the phenolic –OH of **H_2L** to enable as third donor via the phenoxide ion to form **2a** and **4a**. Even then, the expected ruthenium(III) hydrazone chelates **2a** and **4a** were not realised, instead bivalent ruthenium carbonyl complexes **2** and **4** were obtained as sole products in higher yield (47 and 43 % respectively) from the respective precursors. All the complexes **1-4** are quite stable at room temperature, non-hygroscopic and soluble in common organic solvents such as chloroform, dichloromethane, acetonitrile, benzene, DMSO and DMF. The analytical data confirmed the molecular formulae proposed for complexes **1-4**. The IR spectral data of the complexes attested their formation as given in Scheme 1. IR spectrum of the ligand showed a broad band around 3400 cm^{-1}, another sharp band in the region 3200 cm^{-1} due to the presence of OH, NH groups. A very strong band found around 1600 cm^{-1} was assigned to amide carbonyl stretching vibration. But, absence of NH stretching vibrations in addition to the shift in the position of C=O stretching vibrations towards lower wavenumber indicated the embolization of amide oxygen followed by deprotonation prior to coordination with the metal.[24] Interestingly, the band observed around 3400 cm^{-1} owing to the phenolic OH of the ligand moiety remained as such in the spectra of complexes **1** and **3** with a disappearance of the same in complexes **2** and **4.** This feature suggested that phenolic OH is not involved in coordination in the former set of complexes but in the later set.[30] Hence, uni-negative bidentate coordination of **H_2L** in complexes **1** and **3** with deprotonated amide oxygen and imine nitrogen, but a bi-negative tridentate coordination in complexes **2** and **4** through imine nitrogen atom, phenoxide oxygen and deprotonated oxygen were ascertained. A very strong band around 1960 cm^{-1} in the complexes **2** and **4** was undoubtedly assigned to the coordinated carbonyl group in terminal fashion. In addition, vibrations corresponding to the presence of triphenylphosphine also appeared in the expected region. Electronic spectra of all the complexes recorded in DMSO–Tris–HCl buffer solutions and they displayed three to four bands. The bands appearing around 250- 280 nm have been assigned to intra-ligand transitions.[31] The bands around 329-390 nm have been assigned to ligand to metal charge transfer transitions and the band 429-472 nm have been assigned to MLCT transition.[32] ^{1}H NMR spectra of the complexes **2** and **4** exhibited a singlet at δ 8.84 and 8.74 ppm corresponding to the proton attached to azomethine carbon. The higher

chemical shift value of one of the azomethine protons is due to the binding of its nitrogen (C=N) with metal centre. All other aromatic protons corresponding to the ligand as well as triphenylphosphine/arsine were shown complex overlap of signals in the range 7.81-6.81 ppm in both the complexes. ESI-mass spectrum of complexes **1-4** exhibited $[M + H]^-$ peaks at m/z values 986.96, 943.02,1074.85 and 1030.85, respectively (Fig.S1†-Fig.S4†) in good agreement with the proposed molecular formulae.

EPR Study. Low spin d^5 configuration is a good probe for molecular structure and bonding since the observed "g" values are very sensitive to small changes in structural architect of the complex. Room temperature EPR spectra of complexes **1** and **3** recorded at X-band frequency exhibited distinct anisotropic signals with three different g values ($g_x \neq g_y \neq g_z$) in decreasing order of magnitude as shown in Fig.1 and Table1.This type of spectral silhouette is an indication of an octahedral geometry with rhombic distortion due to the asymmetry of electronic environment around paramagnetic Ru(III) centre. Nature of the spectra, position of the lines and the magnitude of "g" vales are comparable with that of other similar low spin Ru(III) Schiff base complexes.[33-35]

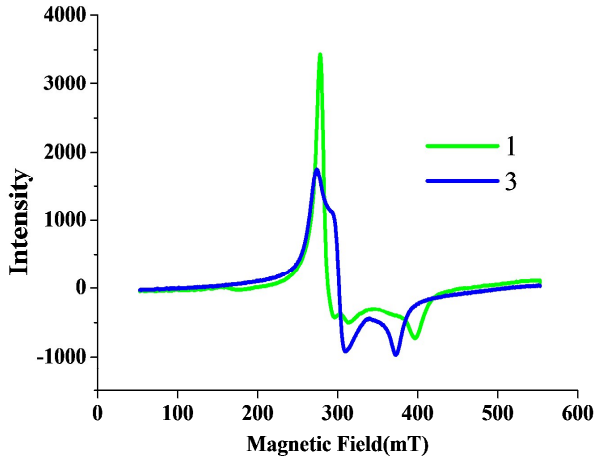

Fig.1 Solid state room temperature EPR spectra of complexes **1** and **3**.

Table 1 EPR spectral data of complexes **1** and **3**

Complex	g_x	g_y	g_z	<g>*
1	2.41	2.24	1.85	2.18
3	2.54	2.22	1.75	2.19

X-ray crystallography. Ruthenium, an iron group metal with various stable oxidation states and could house diverse coordination environment around the metal. Structures of the newly synthesized complexes **1-4** have been established by single crystal X-ray diffraction method and the ORTEP drawings are shown in Fig.2 and 3.The details concerning the data collection and structure refinement of the complexes are summarized in Table 2. Selected bond distances and bond angles with geometrical parameters that are essential for discussion are given in Table 3. With respect to complexes **1** and **3**, the general structural styles are very similar with only slight differences in the geometrical parameters.

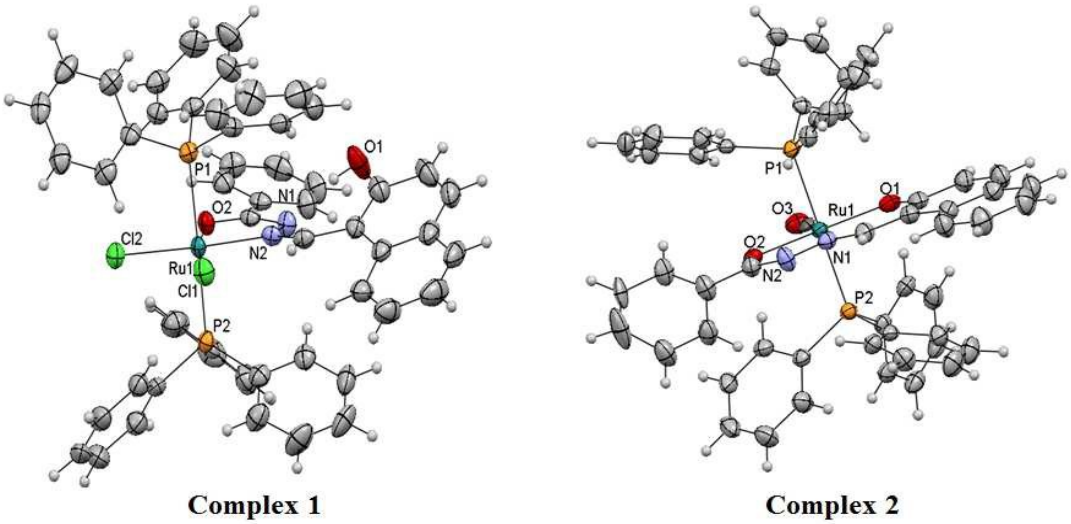

Fig. 2 ORTEP diagram of complexes **1** and **2** with the atom numbering scheme and thermal ellipsoids drawn at 50% probability level.

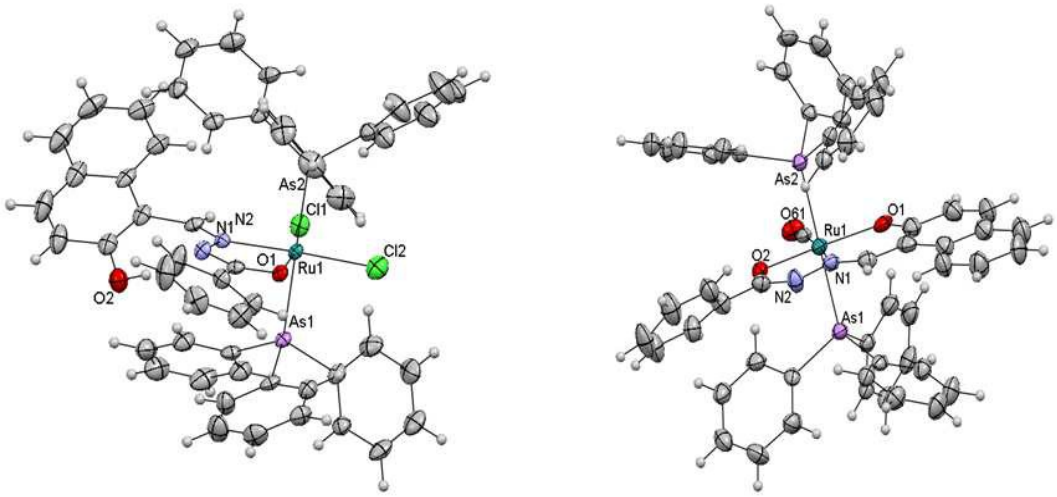

Fig. 3 ORTEP diagram of complexes **3** and **4** with the atom numbering scheme and thermal ellipsoids drawn at 50% probability level.

.

Table 2 Experimental data for crystallographic analyses

	Complex **1**	Complex **2**	Complex **3**	Complex **4**
CCDC deposition no.	897084	897083	897086	932058
Empirical formula	$C_{54}H_{43}Cl_2N_2O_2P_2Ru$	$C_{56}H_{46}N_2O_4P_2Ru$	$C_{56}H_{45}As_2Cl_8N_2O_2Ru$	$C_{56}H_{46}As_2N_2O_4Ru$
Formula weight	985.81	973.96	1312.45	1061.86
Temperature (K)	110(2)	110(2)	110(2)	110(2)
Wavelength (Å)	1.54178	1.54178	0.71073	1.54178
Crystal system	Triclinic	Monoclinic	Triclinic	Monoclinic
Space group	P-1	P2(1)/n	P-1	P2(1)/n
Unit cell dimensions				
a (Å)	11.8342(13)	18.6685(11)	11.8881(8)	18.7940(6)
b (Å)	12.5577(14)	11.8468(7)	12.3931(9)	12.0352(4)
c (Å)	17.382(2)	20.9353(12)	19.70351(14)	20.9907(7)
α (°)	76.856(8)	90	83.282(2)	90
β (°)	86.871(8)	99.018(3)	79.771(2)	99.668
γ (°)	86.714(8)	90	73.680(2)	90
Volume ($Å^3$)	2509.0(5)	4572.9(5)	2734.8(3)	4680.4(3)
Z	2	4	2	4
Density(calculated) (Mg/m^3)	1.305	1.415	1.594	1.507
Abs. coefficient (mm^{-1})	4.430	3.839	1.922	4.675
F(000)	1010	2008	1314	2152
Reflections collected	56569	33592	9544	6932
Independent reflections	7277[R(int) = 0.0626	6708[R(int) = 0.0632]	9544[R(int) =0.0000]	6932[R(int) =0.0000]

Goodness-of-fit on F^2	1.047	1.042	1.080	1.097
Final R indices I>2sigma(I)]	R1=0.0266, wR2=0.0666	R1=0.0331,wR2=0.0758	R1=0.0548,wR2=0.1455	R1=0.0342, wR2=0.0816
R indices (all data)	R1=0.0311, wR2=0.0676	R1=0.0456, wR2=0.0794	R1=0.0685, wR2=0.1536	R1=0.0484, wR2=0.0847

Table 3 Selected Bond Lengths [Å] and Bond Angles [deg] for Complexes **1- 4**

	Complex **1**	Complex **2**	Complex **3**	Complex **4**
Ru(1)-N	2.076(2)	2.036(3)	2.072(4)	2.034(3)
Ru(1)-O(1)		2.087(2)	2.034(4)	2.088(3)
Ru(1)-O(2)	2.029(1)	2.067(2)		2.064(2)
Ru(1)-Cl(1)	2.3428(7)		2.327(1)	
Ru(1)-Cl(2)	2.3392(7)		2.335(1)	
Ru(1)-C		1.911(3)		1.875(4)
Ru(1)-P(1)	2.4165(6)	2.388(8)		
Ru(1)-P(2)	2.4227(7)	2.3769(8)		
Ru(1)-As(1)			2.4779(6)	2.4439(4)
Ru(1)-As(2)			2.4897(6)	2.456(4)
P(1)-Ru(1)-P(2)	178.19(2)	177.87(3)		
As(1)-Ru(1)-As(2)			178.72(2)	176.71(2)
Cl(1)-Ru(1)-Cl(2)	100.59(2)		98.04(5)	
Cl(1)-Ru-N(2)	92.33(5)		93.5(1)	
Cl(2)-Ru(1)-N(2)	167.04(5)		168.5(1)	
N-Ru(1)-O(2)	77.30(7)	78.24(9)	77.0(1)	78.0(1)
N(1)-Ru(1)-O(1)		90.41(9)		90.9(1)
Cl(1)-Ru(1)- O(1)	169.59(5)		170.4(1)	
Cl(2)-Ru(1)-O(2)	89.79(4)		91.5(1)	
C-Ru(1)-O(1)		95.7(1)		94.7(1)
C-Ru(1)-O(2)		95.7(1)		96.4(1)
C-Ru(1)-N(1)		173.8(1)		174.1(1)

Crystal structure of complexes 1 and 3. From the unit cell dimensions, it is clear that the crystals of complexes **1** and **3** are triclinic belonging to the P-1 space group and structure showed that the Ru(III) ion in complex **1** and **3** possessed an octahedral coordination satisfied by Cl_2NOP_2 donors with meridionally spanning imine-N and deprotonated amide oxygen donor atoms of the hydrazone and form a five membered chelate ring and two chloride ions of the starting metal precursor. The remaining apical sites are sated by two triphenylphosphines/triphenylarsines. The distortion from the ideal octahedral geometry in these complexes is due to the small bite angle of the NO chelate of the hydrazone ligand (77.30°/77.0°), the outward bending of the chloride ions Cl1-Ru1-Cl2 (100.59°/98.04°) and also the distortions of the other bond angles from the required 90° and 180° for a perfect

octahedron. The trans Ru-P/Ru-As bond lengths observed (2.416-2.490 Å) in both the complexes are longer than the equatorial bond lengths (2.029-2.343 Å) indicating an axial distortion. This bond lengthening could be attributed to the strong trans influence of the bulkier PPh_3/$AsPh_3$ ligands. This observation is similar to that evidenced by the nature of EPR spectra of the paramagnetic low-spin Ru(III) complexes **1** and **3**. In addition, complex **3** was found to be solvated by two molecules of chloroform. An intramolecular N…H-O hydrogen bonding between the phenolic OH and N2 nitrogen of the ligand moiety was also found in the crystal structure of the complexes **1** and **3**. The Ru–P, Ru-As, Ru–O, Ru–N and Ru–Cl bond lengths found in the complexes agree well with those reported for similar ruthenium(III)complexes.[36-38]

Crystal structure of complexes 2 and 4. Systematic reflection conditions and statistical tests of the data suggested that the crystals of **2** are monoclinic with space group P 21/n. The Ru(II) ion exhibited a hexa-coordination with strained octahedral geometry. The equatorial coordination comes from the imine nitrogen, deprotonated amide-O and phenolic oxygen of the tridentate chelating ligand forming a five and a six membered ring by two ON chelation with bite angles N1–Ru1–O2(78.24°) and N1–Ru1–O1 (90.41°) and a carbonyl carbon. The trans arrangement of bulky PPh_3 ligands may be due to the presence of CO, a stronger π-acidic ligand that completes the hexa coordination.[39] The distorted octahedron is evidenced by the longer Ru-P/Ru-As bonds when compared to the equatorial bonds and also the deviation from the corresponding cis and *trans* bond angles of 90° and 180°. The crystals of complexes **2** and **4** contain a solvated methanol that creates an intermolecular hydrogen bonding between N2 nitrogen of the hydrazone ligand in both the complexes.

Proposed mechanism for the formation of complexes 2 and 4. Complexes **1** & **2a** as well as **3** & **4a** are the expected products of the above represented reaction. However, instead of the formation of **2a** and **4a**, complexes **2** and **4** in which the ruthenium ion was reduced to bivalent oxidation state rather than that of trivalent ruthenium in the starting precursor were quite unexpectedly realised from the appropriate reactions. Interestingly, the formation of Ru-CO bond in complexes **2** & **4** has instigated us to investigate the way for the generation of a carbonyl group. In the literature, it was well established that formaldehyde is used as source for the carbonyl ligand by Ahmed et al.[40] Hence, we felt that *in situ* generation of formaldehyde by ruthenium assisted methanol dehydrogenation (used as solvent) served as a source of carbon monoxide and thus produced complexes **2** and **4**. Further, it is an established fact that carbonyl ligand could stabilize the metal in a zero valent or low positive oxidation

states in metal carbonyls. Earlier reports described that the first generation Grubbs metathesis catalyst with primary alcohols formed ruthenium monohydride monocarbonyl species.[41] Yi, C *et al*. reported that heating Ru(II) and Ru(III) compounds in the presence of primary alcohols formed Ru-CO complexes.[42] Based on the above discussion, we proposed a mechanism in Scheme 2 to account for the formation of complexes **2** & **4** in the absence as well as the presence of a base.

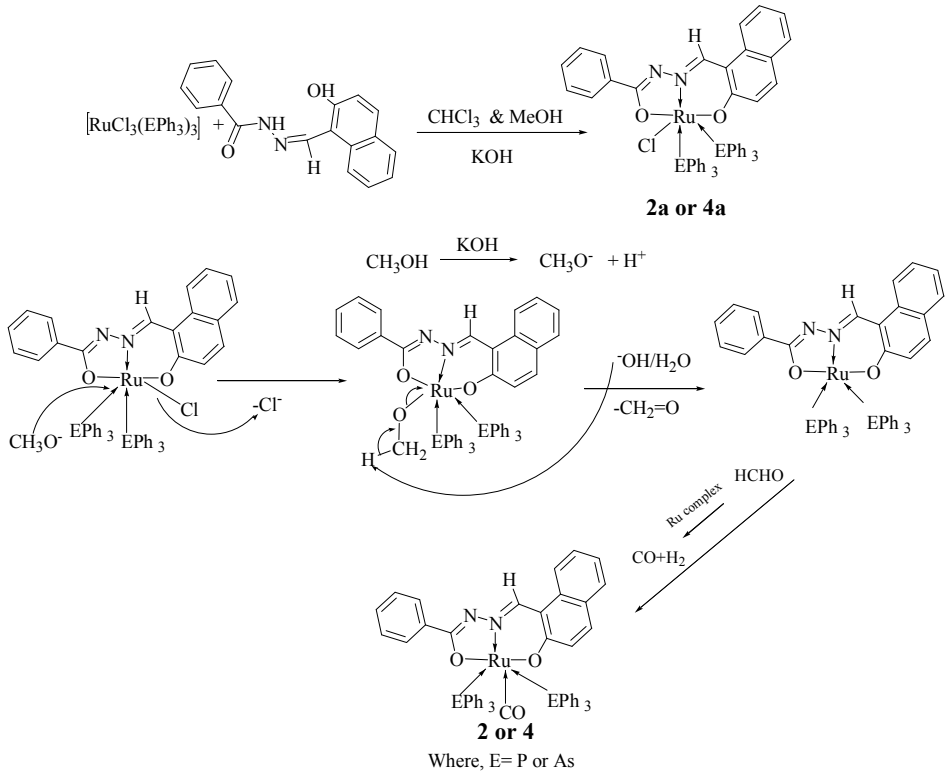

Scheme 2. Proposed mechanism for the formation of complexes **2** and **4.**

DNA binding studies

Absorption spectroscopic measurements. Application of electronic absorption spectroscopy in DNA-binding studies is one of the most useful techniques.[43] Transition metal complexes could bind to DNA via covalent (a labile ligand is replaced with a nitrogen atom of DNA base, such as guanine N7) and/or non-covalent interactions (intercalative, electrostatic and groove binding).[44] A complex that binds to DNA through intercalation involving a strong stacking interaction between an aromatic chromophore and the base pairs of DNA changes the double helix structure of the later and thus usually results in hypochromism. Additionally, the existence of a red shift (bathocromism) is an indication of the stabilization of the DNA duplex.[45,46] The extent of the hypochromism commonly parallels the intercalative binding affinity. Electronic spectra of the complexes **1** -**4** measured in the presence and absence of CT-DNA are given in Fig.4, Fig.S5†and S6†. To investigate the absorptivity changes of the respective complexes upon the incremental addition of DNA, their LMCT transitions observed at 472, 384, 376 and 381 nm were used. The above mentioned absorption bands exhibited varying degrees of hypochromism such as 36.9, 20.3, 22.5 and 18.1% corresponding to complexes **1**-**4**. The intrinsic binding constant, K_b, is a useful tool to monitor and compare the magnitude of the binding strength of compounds with CT-DNA. From the plot [DNA]/[ε_a-ε_f] versus [DNA] (Fig.S7†), K_b values are calculated and are given in Table 4. The overall binding affinity of the complexes is in the order **4** < **2** < **3** < **1**. The binding constant values of complexes **2** and **4** are nearly equal and only a little smaller than that of complex **3**. The observed hypochromism, blue shift and values of K_b revealed that all the complexes bind to DNA via intercalative mode.[47] These results are comparable with those reported earlier for the intercalative mode of various metallointercalators.[24, 48, 49] One potential way to increase the activity of a compound that can coordinate to DNA is to include hydrogen-bonding functionalities on the compound such that both coordination and hydrogen-bonding interactions with DNA can occur. Thus complexes **1** and **3** containing non-coordinated phenolic -OH group could have involved in hydrogen-bonding interactions with DNA to enhance their binding propensity than the complexes **2** and **4** without free hydroxyl group of phenolic moiety.

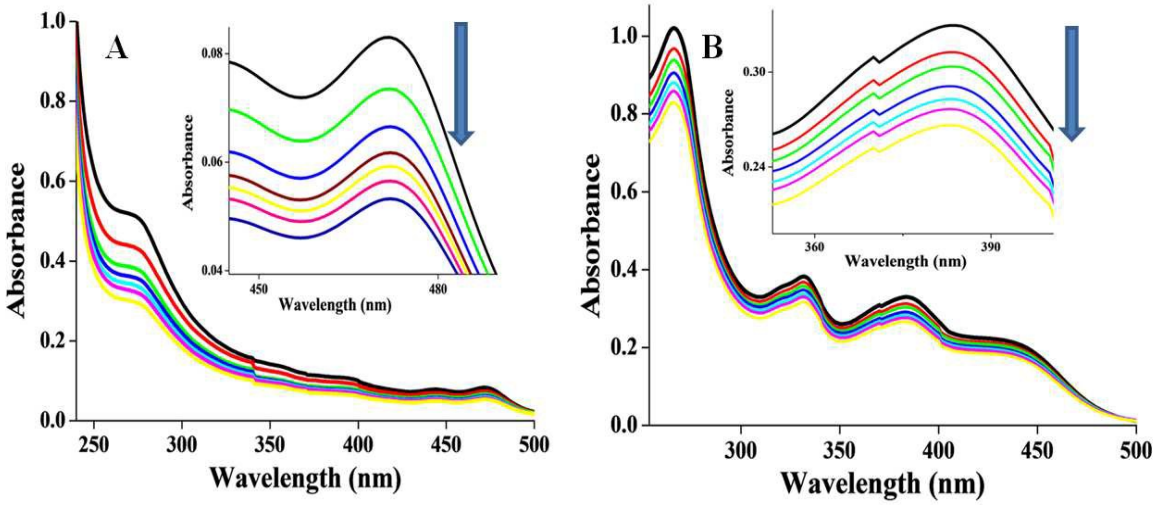

Fig.4 Electronic spectra of complexes **1(A)** and **2(B)** in Tris-HCl buffer upon addition of CT-DNA. [Complex] = 25 μM, [DNA] = 0−20 μM. Arrow shows that the absorption intensities decrease upon increasing DNA concentration.

Table 4 Absorption and emission spectral properties of ruthenium complexes bound to CT-DNA

Complex	$K_b(M^{-1})$	$K_q(M^{-1})$	$K_{app}(M^{-1})$
1	$9.94\pm0.38\times10^4$	$1.09\pm0.41\times10^5$	$2.95\pm0.63\times10^6$
2	$1.34\pm0.11\times10^4$	$1.79\pm0.20\times10^4$	$1.63\pm0.21\times10^6$
3	$1.71\pm0.25\times10^4$	$2.05\pm0.18\times10^4$	$1.62\pm0.11\times10^6$
4	$1.31\pm0.27\times10^4$	$6.55\pm0.67\times10^3$	$6.54\pm0.22\times10^5$

EB-Bound DNA studies. EB, a phenanthridine fluorescence dye is a typical intercalator and emits intense fluorescence around 600 nm due to a strong intercalation of the planar phenanthridinium ring between the adjacent DNA base pairs.[50] Addition of a second molecule that could replace EB from the bound EB-DNA complex could cause a decrease in the intensity of DNA-induced EB emission.[51] As the complexes used in this study are non-fluorescent at room temperature in solution or in the presence of CT-DNA, their binding to DNA could not be evaluated directly through the emission spectra. So EB replacement

studies have been carried out to gain support for the binding of each complex with DNA. The fluorescence emission spectra of EB bound to DNA in the absence and presence of the complexes are shown in Fig.5. From the figure, it is clear that an appreciable reduction in the fluorescence intensity of about 75.9, 53.8, 54.55 and 30.8% together with bathochromic shift of 2, 2, 4 and 1 nm was observed on addition of complexes **1-4** respectively. These results are consistent with the absorption spectral observations. Further, the analysis of the quenching data using Stern–Volmer equation gave the corresponding K_q values and the apparent binding constant (K_{app}) values (Fig. S8† and Table 4). From these values, we can observe that the complexes can effectively replace EB from EB-DNA complex. The binding and quenching constant values increases in the order **4** < **2** < **3** < **1**. The calculated values of K_q and K_{app} are larger than the values reported for few other partial intercalators.[24,13] Further, it is worth to point out here that complexes **1** and **3** containing ruthenium ion in its 3+ oxidation state behaved as better intercalators than that of complexes **2** and **4** in which the metal exists as bivalent cation. Similar observation was already reported in the literature.[52] In addition, the presence of non-coordinated phenolic –OH group in the complexes **1** and **3** could have provided more sites for the interaction of DNA and thus led to higher binding and quenching constants.[53]

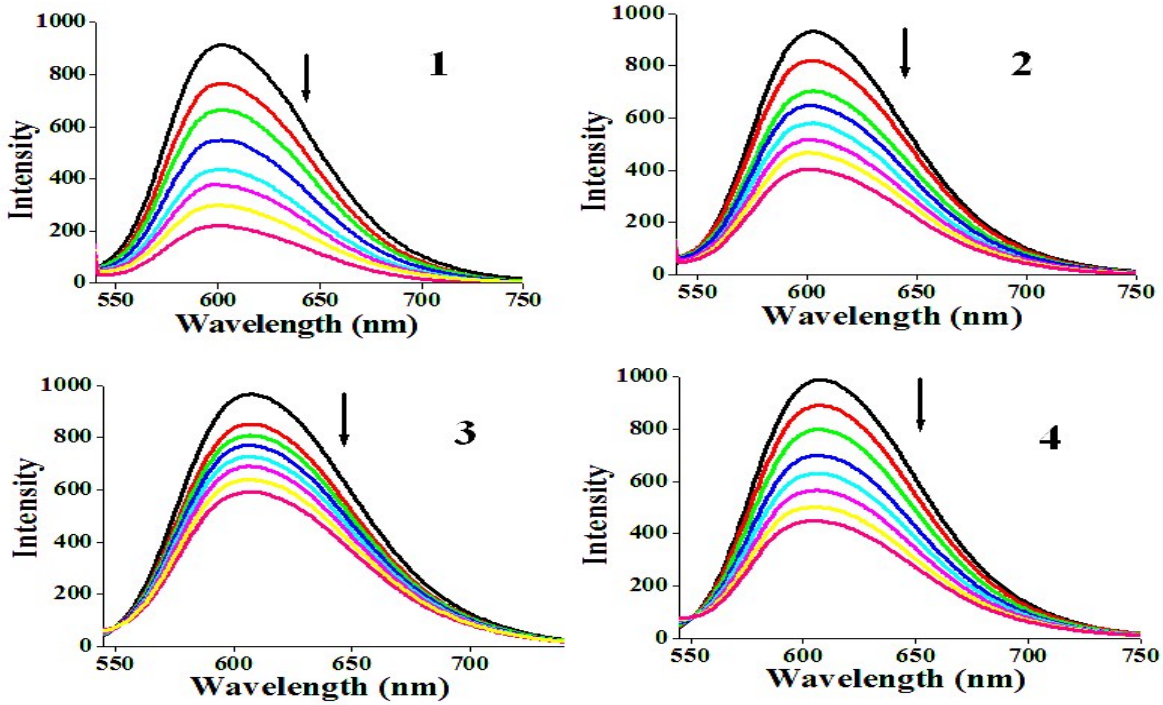

Fig. 5 Emission spectra of the DNA−EB system, λexi = 515 nm, λemi = 530−750 nm, in the presence of complexes **1 - 4**. [DNA] = 10 μM, [Complex] = 0−100μM, [EB] = 10 μM. Arrow shows that the emission intensity changes upon increasing complex concentration.

Protein binding studies

Quenching of BSA fluorescence by Ru(III) and Ru(II) complexes. Interaction of complexes **1 - 4** with BSA was studied by fluorescence spectroscopy using tryptophan emission quenching experiments. Serum albumins are important proteins involved in the transport of amino acids and drug molecules through the blood stream. Binding of a drug to albumin may produce changes of the drug or may give insight about the paths for transportation. Hence, studies on the binding of a drug with a protein will help to understand the uptake and transportation of a drug and to explain the relationship between structures and functions of a protein. Bovine serum albumin (BSA) has been one of the most extensively studied proteins, particularly because of its structural homology with human serum albumin (HSA).[54-57] In order to investigate the binding of complexes **1-4** with BSA, absorption and fluorescence titration experiments were carried out. Fig.S9† shows the emission spectra of BSA in the absence and presence of complexes **1-4**, respectively. In all the experiments, 1 μM BSA was titrated against different concentration of the complexes **1-4** ranging from 0–12μM. Upon an incremental addition of complexes **1-4** to the solution of BSA, about 70%, 55%, 73% and 57% reduction to the initial fluorescence intensity of BSA at 345 nm accompanied by a small red shift of 2, 2, 2 and 4 nm was observed for complexes **1-4** respectively. Such an effective quenching to the intensity of fluorescence emission revealed a strong interaction between the complexes and BSA protein. The magnitude of quenching constant(K_{SV}), binding constant(K_b) values and number of binding sites(n) obtained from Stern-Volmer and Scatchard plots are given in Fig.6 and Table 5. From the values, it is clear that all the complexes interact with BSA strongly and the interaction of complexes **1** and **3** is slightly higher than the other. The values of *n* at room temperature are approximately equal to 1 for both the complexes indicating the existence of single binding site in BSA for the complexes.

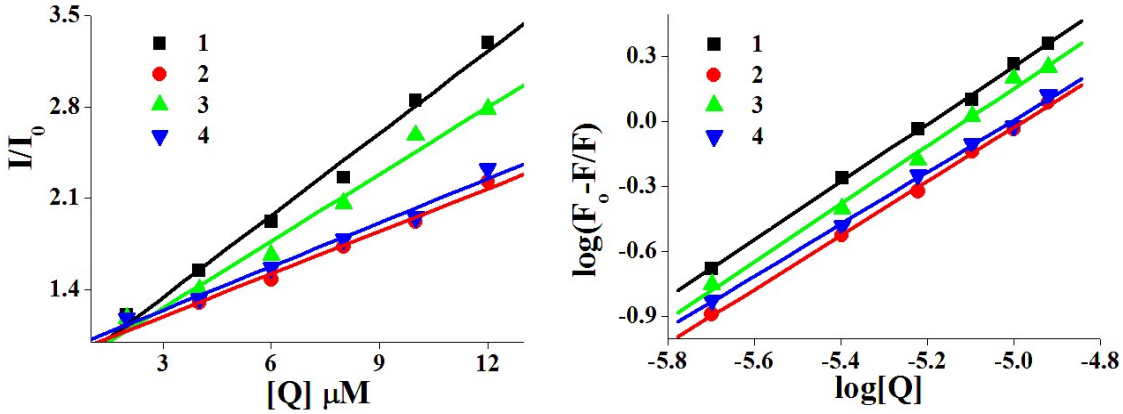

Fig.6 Stern−Volmer (A) and Scatchard (B) plot of the BSA fluorescence titration for complexes **1 - 4**.

Table 5 Emission spectral properties of ruthenium complexes bound to BSA

Complex	$K_{sv}(M^{-1})$	$K_b(M^{-1})$	n
1	$2.09\pm0.65\times10^5$	$7.91\pm0.04\times10^6$	1.3287
2	$1.01\pm0.03\times10^5$	$1.62\pm0.11\times10^6$	1.1081
3	$1.71\pm0.32\times10^5$	$6.44\pm0.23\times10^6$	1.3312
4	$1.12\pm0.07\times10^5$	$1.02\pm0.09\times10^6$	1.2472

It is well known that dynamic quenching affected only the excited state of fluorophores but did not change the absorption spectrum. However, static quenching mechanism due to the formation of a non-fluorescence ground state complex between the fluorophore and quencher affected the absorption spectrum. UV-visible spectra of BSA in the absence and presence of the complexes **1-4** in Fig.S10 † showed that the absorption intensity of BSA was enhanced as the complexes were added and a little blue shift was observed. This shows the operation of static quenching mechanism as reported earlier.[58]

Synchronous spectral studies. Synchronous fluorescence spectra provide information on the molecular micro-environment, particularly in the vicinity of the fluorophore functional groups. BSA contains three fluorophores, namely, tryptophan, tyrosine and phenylalanine. Among them, tryptophan is the most dominant fluorophore, located at the substrate binding sites and then the tyrosine residue. The study of their interactions with small molecules can provide useful insights to understand the molecular micro-environment. Moreover, there is evidence of conformational changes of serum albumin induced by its interaction with low molecular weight drugs, which appear to affect secondary and tertiary structures of

proteins.[55,59,60] Synchronous method is usually applied to find out the conformational changes in the active binding sites of the protein that is around the tryptophan and tyrosine region. Hence, the synchronous fluorescence spectra of BSA were measured before and after the addition of test compounds to get valuable information on the structural changes and molecular micro-environment. According to the theory of Miller, when the D-value ($\Delta\lambda$) between excitation and emission wavelength are stabilized at 15 or 60 nm, the synchronous fluorescence gives the characteristic information of tyrosine or tryptophan residues.[61]

The synchronous fluorescence spectra of both tyrosine and tryptophan residues present in BSA were shown (Fig.S11† and Fig.S12†) with respect to various concentrations of ruthenium(II) and ruthenium(III) hydrazone complexes added.

After the addition of complexes **1**, **2**, **4** to BSA, a slight decrease in the intensity of tyrosine residue along with a red shift of 8, 8 and 4 nm was observed in the fluorescence spectra respectively. In contrast, addition of complex **3** to BSA slightly increased the intensity of the band with a red shift accounting for 8 nm. However, addition of ruthenium hydrazone complexes to BSA caused very small change in the environment around the tyrosine residue. When Ru(III) and Ru(II) hydrazone complexes were added to BSA solution, a significant decrease in the intensity of tryptophan fluorescence emission was observed with 2 nm red shift in all the cases. These observations do specify that the complexes **1-4** did not show pronounced effect on the micro-environment of tyrosine residues during the binding process but to a larger extent at the tryptophan micro-environment. The interaction of ruthenium hydrazone chelates with tryptophan residue led to a decrease in the polarity of the fluorophore by increasing the hydrophobicity around it. The magnitude of binding interaction between the complexes and BSA suggest that they can easily be stored in protein and released at desired target areas.

The calculated values of the DNA/BSA binding constant and quenching constants of the complexes **1-4** suggested that complexes **1** and **3** possess strong interaction with biomolecules than complexes **2** & **4** under identical conditions**.** The superior performance exhibited by the former pair of complexes may be attributed to the presence of a trivalent ruthenium ion containing the hydrazone moiety in which the phenolic oxygen remains uncoordinated and thus readily available for H-bonding with biomolecules than the later pair of complexes containing a bivalent ruthenium ion in their architect coordinated with the same

ligand but devoid of a free hydroxyl group that can promote hydrogen bonding interactions with biomolecules.

Cytotoxicity studies

Effect of Ru(III) and Ru(II) complexes on cell proliferation. The significant results of the DNA/protein binding analysis results motivated us to proceed further on the exploration of their *in vitro* cytotoxicity on A549 cell lines. *In vitro* anti-proliferative potential of the complexes **1-4** were tested against A549 cell line using MTT assay in a time and dose dependent fashion. For an incubation period of 12 and 24 h, there were no substantial reduction in cell proliferation by the complexes when compared with control cells, but at 48 h incubation time, the complexes showed significant reduction in the cell viability and that was selected as optimum time period. The dose dependent cell death inducing ability of the complexes has been investigated by using the percentage cell growth inhibition *versus* complex concentration plot. Among the complexes, complex **1** was more effective with the IC_{50} value of 18±0.67 μM than the other complexes **2**(24±1.0 μM), **3**(22±1.17 μM) & **4** (24±0.93μM). It is important to mention that the all the complexes showed better growth inhibitory effect than the well-known anticancer drug cisplatin with the IC_{50} value of 25 μM. The lower IC_{50} value of all the complexes than cisplatin and some of the ruthenium complexes from the literature [62, 63] made us to further explore their cytotoxic potential. It has been proved that the ligands with potential hydrogen bonding nature could enhance their cytotoxicity through strong interaction with biomolecules such as DNA/protein.[64] Thus complexes **1** and **3** with sites for intramolecular hydrogen bonding through free phenolic –OH displayed superior cytotoxic activity than complexes **2** and **4**.

LDH Assay. LDH is a stable cytoplasmic enzyme that catalyses the oxidation of lactate and the reduction of pyruvate. This enzyme is a well-known marker released into the culture medium due to loss of membrane integrity resulting from apoptosis of cells and controls important biochemical reactions. Hence, LDH release is used to analyse the drug induced cytotoxicity of cancer cells.[65, 66] In this, IC_{50} concentration of the complexes **1-4** were added and treated for 48 h with A549 cell lines, significant level of LDH leakage was observed in the cell culture medium that is an indication of loss of membrane integrity resulting from apoptosis of cells (Table 6).

Nitric oxide assay. Nitric oxide (NO) is an important biological messenger molecule that exerts diverse physiological and pathological functions such as blood flow regulation, signal transduction and immune defence.[67] Nitric oxide, a reactive short lived free radical produced non-enzymatically during oxidative stress rapidly reacts with ROS and thus causes the production of several RNS that potentiate damage in most of the biomolecules including DNA and protein.[68] Among the other mediators of apoptosis, nitric oxide play crucial role to induce apoptosis in numerous cell types.[69-72] Hence, the newly synthesized bivalent and trivalent ruthenium complexes were tested for their potential to enhance the level of NO in A549 cell line. A significant enhancement in the level of nitrite was found in the cells treated with complexes **1-4** when compared to control cells (Table 6). Predominantly, complexes **1** and **3** were more effective to enhance the level of NO than the others in the culture medium and hence confirmed their cytotoxic potential.

Table 6 LDH and nitrite released by A549 cell lines after an incubation period of 48h with with IC_{50} concentration of complexes **1-4.**

Complex	**LDH released (%)**	**Nitrite released (nano moles)**
Control	0	0.80±0.11
1	54±2.3	10±0.37
2	24.13±1.2	8±0.29
3	45±1.6	9±0.4
4	22±0.7	6 ±0.24

ROS Assay. ROS are constantly generated as a natural by-product in multiple pathways including both enzyme-catalyzed and non-enzymatic reactions and have important roles in cell signalling and homeostasis.[73] The role of ROS as mediators of apoptosis is becoming increasingly recognized. Many potential anticancer and chemo preventive agents induce apoptosis through ROS generation.[74,75] To investigate the cell death induced by the test compounds were dependent on the level of ROS, the IC_{50} concentration of test compounds were treated with A549 cells for 15, 30 and 60 min duration and the change in intensity of DCF fluorescence emission with respect to different incubation time is presented in Fig.9. The DCF fluorescence intensity increased linearly with respect to time upon treatment with complexes and hence proved the capability of the complexes to enhance the oxidative stress in A549 and thus promote apoptosis.

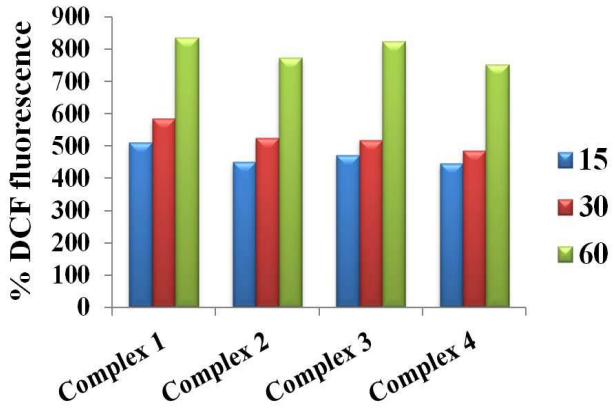

Fig. 7 Time dependent effect of ruthenium complexes on reactive oxygen species generation.

PI Staining assay. Design of chemotherapeutic drugs in order to understand the complexities of apoptosis evolved by cancer cells and development of strategies to selectively induce apoptosis in cancer cells have turned into a unique target in cancer drug development.[76] Many compounds can kill cancer cells through apoptic pathway. Apoptotic cell death pattern has distinct morphological and biochemical features shows nuclear shrinkage, cytoplasmic membrane blebbing etc.[77] PI staining is sensitive to DNA and was used to analyse changes in the nuclear morphology to assess the type of cell death induced by the complexes. Hence, A549 cell lines were treated with known IC_{50} concentration of the complexes **1** - **4** followed by PI staining**.** After the treatment of cells with the complexes for 48 h, selective images taken by an inverted microscope are shown in Fig.10.The chromatin condensation, nuclear shrinkage, and plasma membrane blebbing were observed using fluorescence microscope those are the clear indication of apoptic cell death pattern.

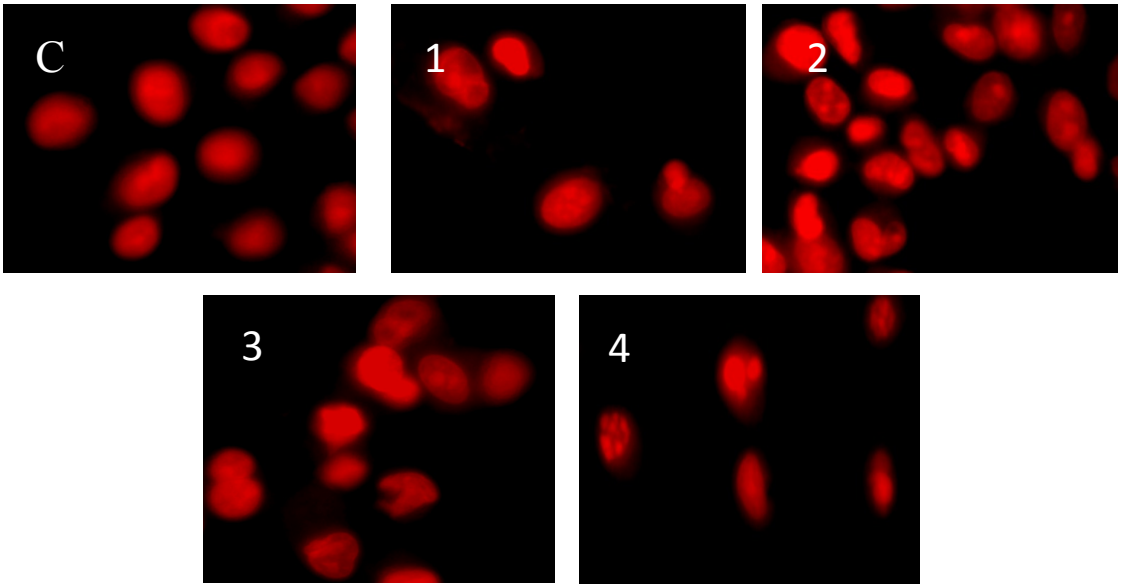

Fig.8 PI staining images of DNA damage in A549 cells after treatment with ruthenium complexes (C-control, 1- complex **1**, 2**-** complex **2**, 3- complex **3** and 4- complex **4)**

Conclusion

Reactions of trivalent ruthenium precursors $[RuCl_3(EPh_3)_3]$ (where E = P or As) with 2-hydroxy naphthaldehyde benzoic acid hydrazone (H_2L) yielded a mixture of bivalent and trivalent ruthenium complexes. However, the same reaction in presence of a base led to the exclusive formation of appropriate bivalent ruthenium complexes. A suitable mechanism based on the decomposition of Grubbs metathesis catalysts and alcohol dehydrogenation is proposed to understand the formation of bivalent ruthenium complexes as a minor or sole product in the absence/presence of a base. Intercalative binding interaction of these with CT-DNA was ascertained by absorption and emission titrations. BSA interaction potential of the complexes determined by fluorescence quenching experiments vindicates a strong interaction between the complexes and biomolecule to alter the conformation of later. All the complexes underwent quenching by static quenching mechanism. Synchronous spectral studies of the complexes with BSA revealed significant interaction with the tryptophan microenvironment than the tyrosine present in the protein. In vitro cell proliferation assay supported their notable cytotoxic nature with few micromolar IC_{50} value against A549 cell line. The DNA/Protein binding and cytotoxic potential of the complexes decreased in the order **1**>**3**>**2**>**4**. Enhanced release of LDH, NO and ROS from A549 cells observed upon treatment with IC_{50} concentration of the complexes revealed an interaction between the complexes and

DNA/protein of the cancer cells and thus arrested their growth by triggering apoptosis as identified from the cell morphologies through PI staining assay. Combination of the biological prospective associated with bivalent as well as trivalent ruthenium complexes did throw some light on the influence of structure and oxidation state of the metallo-drugs on their bio-activity. Specifically, trivalent ruthenium complexes possessing uni-negative bidentate chelation of the hydrazone with phenolic oxygen uncoordinated had offered effective sites for hydrogen bonding interaction with biomolecules and made them as better candidates than that of bivalent ruthenium complexes possessing the same ligand as a bi-negative tridentate donor by utilizing the deprotonated phenolic oxygen also for coordination with the metal. Among the trivalent ruthenium hydrazone complexes, the one containing triphenylphosphine as a co-ligand exhibited superior performance than its arsine counterpart.

Acknowledgement

The corresponding author of the manuscript (N. D.) acknowledges the Council of Scientific and Industrial Research (CSIR), Government of India, New Delhi, for financial support in the form of a major research project (CSIR Sanction letter no. 01(2684)/12/EMR-II dated 03.10. 2012) and for the award of Senior Research Fellowship (SRF) to one of the authors (E. J.).

References

1 G. Li, T. Bell and E. J. Merino, *Chem. Med. Chem.,* 2011, **6**, 869–875.

2 A.R. Jones, T.R. Bell-Horwath, G. Li, S.M. Rollmann, and E.J. Merino, *Chem. Res. Toxicol.,* 2012, **25**, 2542–2552.

3 (a) M. Bacac, M. Vadori, G. Sava and S. Pacor, *Cancer Immunol.Immunother.,* 2004, **53**, 1101−1110. (b) A. Bergamo, M. Cocchietto, I. Capozzi, G. Mestroni, E. Alessio and G. Sava, *Anti-Cancer Drugs*, 1996, **7**, 697−702. (c) M. Cocchietto, S. Zorzet, A.Sorc and G. Sava, *Invest. New Drugs,* 2003, **21**, 55−62. (d) F. Frausin, V. Scarcia, M. Cocchietto, A. Furlani, B. Serli, E. Alessio and G. Sava, *J. Pharmacol. Exp. Ther.,* 2005, **313**, 227−233. (e) S. Pacor, S. Zorzet, M. Cocchietto, M. Bacac, M.Vadori, B. Turrin, C. Gava, A. Castellarin and G. Sava, *J. Pharmacol. Exp. Ther.,* 2004, **310**, 737−744. (f) G.Pintus, B. Tadolini, A. M. Posadino, B. Sanna, M. Debidda, F. Bennardini, G. Sava and C. Ventura, *Eur. J. Biochem.,* 2002, **269**, 5861−5870. (g) G. Sava, E. Alessio, A. Bergamo and G. Mestroni, *Top. Biol. Inorg. Chem.,*1999, **1**, 143−169. (h) G. Sava, K. Clerici, I. Capozzi, M. Cocchietto, R. Gagliardi, E. Alessio, G. Mestroni and A. Perbellini, *Anti-Cancer Drugs*, 1999, **10**, 129−138. (i) S. Zorzet, A. Bergamo, M. Cocchietto, A. Sorc, B.

Gava, E. Alessio, E. Iengo and G.Sava, *J.Pharmacol. Exp. Ther.,* 2000, **295**, 927−933. (j) S. Zorzet, A. Sorc, C. Casarsa, M. Cocchietto and G. Sava, *Met.Based Drugs*, 2001, **8**, 1−7.

4 (a) A. Bergamo and G. Sava, *Dalton Trans*., 2007, 1267−1272. (b) B. Gava, S. Zorzet, P. Spessotto, M. Cocchietto and G. Sava, *J. Pharmacol. Exp. Ther*., 2006, **317**, 284−291. (c) G. Sava, S. Zorzet, C.Turrin, F. Vita, M. Soranzo, G. Zabucchi, M. Cocchietto, A. Bergamo, S. DiGiovine, G. Pezzoni, L. Sartor and S. Garbisa, *Clin. Cancer Res.,* 2003, **9**, 1898−1905.

5 B. Wu, M.S. Ong, M. Groessl, Z. Adhireksan, C.G. Hartinger, P. J. Dyson and C.A. Davey, *Chem. Eur. J.,* 2011, **17**, 3562−3566.

6 S. Dhar, S. J. Lippard and E. Alessio, *In Bioinorganic Medicinal Chemistry,* 2011, 79−95.

7 B. P. Esposito and R. Najjar, *Coord. Chem. Rev.,* 2002, **232**, 137-149.

8 (a) N.A. Kratochwil, W. Huber, F. Muller, M. Kansy and P.R. Gerber, *Biochem. Pharmacol*., 2002, **64**, 1355–1374. (b) G. Colmenarejo, *Med. Res. Rev*., 2003, **23**, 275–301.

9 F. J. Kratz, *Control. Release*, 2008, **132**, 171–183.

10 (a) A. Levina, A. Mitra and P.A Lay, *Metallomics,* 2009, **1**, 458–470. (b) W. H. Ang and P. J. Dyson, *Eur. J. Inorg. Chem*., 2006, **20**, 4003–4018. (c) J. Costa Pessoa and I. Tomaz, *Curr. Med. Chem*., 2010, **17**, 3701–3738.

11 (a) C. Tan, S. Lai, S. Wu, S.Hu, L. Zhou, Y. Chen, M. Wang, Y. Zhu, W. Lian, W. Peng, L.Ji and A.Xu, *J. Med. Chem.,* 2010, **53**, 7613–7624.(b) S. J. Dougan, A. Habtemariam, S.E. McHale, S. Parsons and P. J. Sadler, *Proc. Natl. Aacad. Sci.,U.S.A.* 2008, **105**, 11628-11633.

12 (a) R. Sevim and G. S. Kucukguzel, *Molecules,* 2007, **12**, 1910-1939. (b) D. R. Phillips, R.T. C. Brownlee, J. A. Reiss and P. A. Scourides, *Invest. New Drugs*, 1992, **10**, 79-88. (c) S. Claudia, B. Loretta, M. Stefano, Z. Giuseppe, B. Christian, M. Ernesto, C. Giovanni and P. Manlio, *Mol. Pharmacol.,* 1998, **54**, 1036–1045. (d) J. Easmon, G. Purstinger , K.S. Thies, G. Heinisch and J. Hofmann , *J. Med. Chem.,* 2006, **21**, 6343-6350. (e) T.B. Chaston, R. N. Watts, J. Yuan and D.R. Richardson, *Clin. Cancer Res.,* 2004, **10**, 7365–7374.

13 (a) M. Alagesan, P. Sathyadevi, P. Krishnamoorthy, N. S. P. Bhuvanesh and N. Dharmaraj, *Dalton Trans.,* 2014, **43**, 15829-15840.(b) D.S. Raja, N.S.P. Bhuvanesh and K. Natarajan, *Eur. J. Med. Chem*., 2012, **47**, 73-85.

14 (a) R. Raveendran and S. Pal, *Inorg. Chim. Acta*, 2006 **359**, 3212–3220.(b) R.

Raveendran and S. Pal, *Polyhedron*, 2005, **24**, 57–63.(c) R. Raveendran and S. Pal, *Polyhedron*,2008,**27**, 655–662. (d)A. Mori, T. Suzuki, Y. Sunatsuki, A. Kobayashi, M.Kato, M. Kojima and K. Nakajima, *Eur. J. Inorg. Chem.* 2014, 186–197. (e) A. Mori, T. Suzuki, Y. Sunatsuki, M. Kojima and K. Nakajima, Bull. Chem. Soc. Jpn., 2015,**88**, 480 – 489.

15 J. Chatt, G.J. Leigh, D.M.P. Mingos and R.J. Paske, *J .Chem. Soc A*., 1968, 2636-2641.

16 R. K. Poddar, I. P. Khullar and U. Agarwala, *Inorg. Nucl. Chem. Lett.,* 1974, **10**, 221–227.

17 P. Sathyadevi, P. Krishnamoorthy, R. R.; Butorac, A. H. Cowley, N. S. P. Bhuvanesh, and N. Dharmaraj, *Dalton Trans*., 2011, **40**, 9690–9702.

18 APEX2 *"Program for Data Collection on Area Detectors", Bruker AXS Inc., Madison,* WI 53711-5373, USA.

19 G. M. Sheldrick, *XS, BRUKER AXS Inc., Acta Crystallogr.,Sect. A: Fundam. Crystallogr.,* 2008, **64**, 112–122.

20 A. L. Spek, J. *Appl. Crystallogr.,* 2003, **36**, 7–13.

21 O. V. Dolomanov, L. J. Bourhis, R. J. Gildea, J. A. K. Howard and H. Puschmann, *J. Appl. Crystallogr.,* 2009, **42**, 339–341.

22 J. Marmur, *J. Mol.Biol*., 1961, **3**, 208-218.

23 E. Ramachandran, D.S. Raja, N. P. Rath and K. Natarajan, *Inorg. Chem*., 2013, **52**, 1504−1514.

24 P. Sathyadevi , P. Krishnamoorthy , N.S.P. Bhuvanesh, P. Kalaiselvi , V. Vijaya Padma and N. Dharmaraj, *Eur. J. Med. Chem*., 2012, **55**, 420-431.

25 P. Sathyadevi , P. Krishnamoorthy, R.R. Butorac, A.H. Cowley and N. Dharmaraj, *Metallomics*, 2012, **4**, 498-511.

26 T. J. Mosmann, *J. Immunol. Methods,* 1983, **65**, 55–63.

27 W.E.C. Wacker, D.D. Ulmer and B.L. Vallee, *J. Med.,* 1956, **255**, 449–456.

28 D.J. Stuehr and M.A. Marletta, *J. Immunol*., 1987, **139**, 518–525.

29 H. Wang and J.A. Joseph, *Free Rad. Biol. Med.,* 1999, **27**, 612–616.

30 P. Kalaivani, R. Prabhakaran, P. Poornima, F. Dallemer, K. Vijayalakshmi, V. Vijaya Padma and K. Natarajan, *Organometallics,* 2012, **31**,8323−8332).

31 A. Castineiras and R. Pedrido, *Dalton Trans.,* 2012, **41**, 1363-1372.

32 (a) A.B.P. Lever, *Inorganic Electronic Spectroscopy, 2nd ed., Elsevier, New York,* 1984;(b) G. Csjernyik, A.H. Ell, L. Fadini, B. Pugin and J. Backvall, *J. Org. Chem.,*

2003,**67**, 1657-1662; (c) R. Ramesh and M. Sivagamasundari, *Synth. React. Inorg. Met. Org. Chem.,* 2003, **33**, 899-910; (d) H.S. Abbo, S.J.J. Titinchi, R. Prasad and S. Chaand, *J. Mol. Catal. A: Chem.,*2005, **225**, 225-232.

33 F.A. Cotton, M. Matusz and R.C. Torralba, *Inorg. Chem*., 1989, **28**, 1516–1520.

34 D. Kanchana and R. Ramesh, *Spectrochim. Acta Mol. Biomol. Spectros.,* 2014, **117**, 138–143.

35 N. Raja R. Ramesh and L.Yu, *Polyhedron*, 2012, **31**, 196–201.

36 R. Prabhakaran, P. Kalaivani, R. Jayakumar, M. Zeller, A. D.Hunter, S. V. Renukadevi, E.Ramachandran and K. Natarajan, *Metallomics,* 2011, **3**, 42–48.

37 D. Sukanya, R. Prabhakaran and K. Natarajan, *Polyhedron,* 2006, **25**, 2223–2228.

38 N. Chitrapriya, V. Mahalingam, M. Zeller, R. Jayabalan , K. Swaminathan and K. Natarajan, *Polyhedron,* 2008, **27**, 939–946.

39 K.T. Sathiya, N. Chitrapriya, H. Lee, C.F. Fronczek, F.R. Fronczek and K. Natarajan, *Dalton Trans.,* 2012, **41**, 2066–2077.

40 N. Ahmed, J.J. Levison, S.D. Robinson and M.F. Uttley. *Inorg. Synth.,* 1974, **15**, 48.

41 M. B. Dinger and J. C. Mol, *organometallics,* 2003, **22**, 1089-1095.

42 C. S. Yi, D. W. Lee and Y. Chen, *Organometallics***,** 1999**, 18**, 2043-2045.

43 J.K. Barton, J.J. Dannenberg and A.L. Raphael, *J. Am. Chem. Soc*., 1984, **106**, 2172–2176.

44 Q. Zhang, J. Liu, H. Chao, G. Xue and L. Ji, *J. Inorg. Biochem*., 2001, **83**, 49–55.

45 E. K. Efthimiadou, A. Karaliota and G. Psomas, *J. Inorg. Biochem*., 2010, **104**, 455–466.

46 E. C. Long and J. K. Barton, *Acc. Chem. Res*., 1990, **23**, 271–273.

47 A. Wolf, G. H. Shimer and T. Meehan, *Biochemistry*, 1987, **26,** 6392–6396.

48 S. Arounaguiri and B. G. Maiya, *Inorg. Chem*., 1999, **38**, 842-843.

49 M. K. Tanimoto, K. Dias, S. Dovidauskas and S. Nikolaou, *J. Coord. Chem.,* 2012, **65**, 1504-1517.

50 Q. Zhang, F. Zhang, W. Wang and X. Wang, *J. Inorg. Biochem*., 2006, **100**, 1344–1352.

51 B.C. Baguley and M. Lebret, *Biochemistry,* 1984, **23**, 937–943.

52 N.P. Mohan, N.J. Hardik and R.P. Chintan, *J. Chem. Sci.,* 2014, **126**, 739–749.

53 E. Jayanthi, S. Kalaiselvi, V. Vijaya Padma, N.S.P. Bhuvanesh and N. Dharmaraj, *Inorg.Chim.Acta*, 2015, **429**, 148–159.

54 M.S.; Fasanol, E. Curry, M. Terreno, G. Galliano, P. Fanali, S. Narciso and P. A. Notari, *IUBMB Life*, 2005, **57**, 787-796.

55 D.C. Carter and J.X. Ho, *Adv. Protein Chem.,*1994, **45**,153-203.

56 X.M. He and C.D. Carter, *Nature*, 1992, **358**, 209-215.

57 T. Peters, *Advances in Protein Chemistry*, 1985, **37**, 161-245.

58 P. Krishnamoorthy, P. Sathyadevi, R.R. Butorac, A. H. Cowley and N. Dharmaraj, *Eur. J. Med. Chem*., 2011, **46**, 3376-3387.

59 Y. Wang, H. Zhang, G. Zhang, W. Tao and S. Tang, *J. Lumin*., 2007, **126**, 211–218.

60 B. Priyanka, M. Niharendu and H. Mintu, *J. Agric. Food Chem*., 2012, **60**, 3727−3734.

61 Z. Goldouzian, F. Goldouzian, M. Momen-Heravi, J. Chamani, *Chemical Health Risks*, 2011, 13-15.

62 C.A.S.T. Vilanova-Costa, H.K.P. Porto, F.C. Pereira, A. P. Lima, W.B. Santos and E.P. Silveira-Lacerda, *Biometals*, 2014, **27**, 459-469.

63 A. P. Lima, F.C. Pereira, C.A.S.T. Vilanova-Costa, J.R. Soares, L.C.G. Pereira, H.K.P. Porto, L.A. Pavanin, W.B. Santos and E.P. Silveira-Lacerda, *Biol. Trace Elem. Res*., 2012, **147**, 8-15.

64 F.J. K. Rehmann, L. P. Cuffe, O. Mendoza, D. K. Rai, N. Sweeney, K. Strohfeldt, W. M.Gallagher and M. Tacke, *Appl. Organomet. Chem*., 2005, **19**, 293-300.

65 C. Legrand, J.M. Bour, C. Jacob, J. Capiaumont, A. Martial, A. Marc, M. Wudtke, G. Kretzmer, C. Demangel, D. Duval and J. Hache, *J. Biotechnol*., 1992, **25**, 231-243.

66 E. Bonfoco, D. Krainc, M. Ankarcrona, P. Nicotera and S.A. Lipton, *Proc. Natl. Acad. Sci*., 1995, **16**, 7162-7166.

67 H. W. Schmidt and U. Walter, *NO at work, Cell*, 1994, **78**, 919-925.

68 L. Yu, P.E. Gengaro, M. Niederberger, T.J. Burke and R.W. Schriert, *Proc. Natl. Acad. Sci*., 1994, **91**, 1691-1695.

69 J.E. Albina, B.A. Martin, W.L.J. Henry, C.A. Louis and J.S. Reichner, *J. Immunol*., 1996, **157**, 279-283.

70 J.E. Albina and J.S. Reichner, *Cancer Metastasis Rev*. 1998, **17**, 39-53.

71 U.K. Messmer and B. Brune, *J. Biochem*., 1996, **319**, 299-305.

72 B. Brune, C. Gotz, U.K. Messmer, K. Sandau, M.R. Hirvonen and E.G. Lapetina, *J. Biol. Chem*., 1997, **272**, 7253-7258.

73 T.P.A. Devasagayam, J.C. Tilak, K.K. Boloor, K.S. Sane, S. Ghaskadbi Saroj and R.D. Lele, *J. Assoc. of Physicians of India,* 2004, **52**, 796-804.

74 A. Kawiak, J. Zawacka-Pankau, A. Wasilewska, G. Stasilojc, J. Bigda and E. Lojkowska, *J. Nat. Prod*., 2012, **75**, 9-14.

75 P. Helene, C. Dennis and H. Peng, *Drug. Resist*., 2004, **7**, 97-110.

76 S. Kasibhatla, and B. Tseng, *Mol. Cancer Ther*., 2003, **2**, 573-580.

77 J.F. Kerr, *Toxicol*., 2002, **181**, 471-474.

Supporting Information

ESI-mass spectra of all the four complexes (Fig. S1 - S4†), electronic spectra of complexes **3** and **4** in Tris-HCl buffer upon addition of CT-DNA (Fig. S5† and S6†), [DNA]/[ε_a-ε_f] versus [DNA] plot (Fig. S7†), Stern-Volmer plot (Fig. S8†), emission spectra of BSA (1 μM) in the presence of increasing amounts of complexes **1**, **2**, **3**, and **4** (0−12 μM) (Fig. S9†), absorption titration of complexes with BSA (Fig. S10†) and synchronous spectra of BSA (1 μM) in the presence of increasing amounts of complexes **1**, **2**, **3**, and **4** (0−12 μM) in the wavelength difference of $\Delta\lambda$ = 15 nm and $\Delta\lambda$ = 60 nm (Fig.S11† and S12†). This material is available free of charge via the Internet at http://pubs.acs.org. Crystallographic data for the structures reported in this paper have been deposited with the Cambridge Crystallographic Data Centre (CCDC) as supplementary publication numbers CCDC-897084, 897083, 897086 and 932058 for the ruthenium complexes **1**−**4**. Copies of the data can be obtained free of charge from the CCDC (12 Union Road, Cambridge CB2 1EZ, U.K.; Tel: +44−1223−336408; Fax: +44−1223−336003; Email: deposit@ccdc.cam.ac.uk; Web site: http://www.ccdc.cam.ac.uk).

Table captions

Table 1 EPR Spectral data of complexes **1** and **3**

Table 2 Crystal data and structure refinement of complexes **1-4**

Table 3 Selected bond lengths and bond angles of complexes **1-4**

Table 4 Absorption and steady state emission spectral properties of ruthenium complexes bound to CT-DNA

Table 5 Quenching constant (K_q), binding constant (K_{bin}) and number of binding sites (n) for the interaction of complexes with BSA

Table 6 LDH and nitrite released by A549 cell lines after an incubation period of 48h upon treatment with IC_{50} concentration of complexes **1-4.**

Schemes

Scheme 1 Synthesis of ruthenium hydrazone complexes **1-4.**

Scheme 2 Mechanism for the formation of complexes **2** and **4.**

Figure captions

Fig. 1 Solid state room temperature EPR spectra of the complexes **1** and **3**.

Fig. 2 ORTEP diagram of complexes **1** and **2** with the atom numbering scheme and thermal ellipsoids drawn at 50% probability level.

Fig. 3 ORTEP diagram of complexes **3** and **4** with the atom numbering scheme and thermal ellipsoids drawn at 50% probability level.

Fig. 4 Electronic spectra of complexes **1** and **2** in Tris-HCl buffer upon addition of CT-DNA. [Complex] = 25 μM, [DNA] = 0−20 μM. Arrow shows that the absorption intensities decrease upon increasing DNA concentration.

Fig.5 Emission spectra of the DNA−EB system, λexi = 515 nm, λemi = 530−750 nm, in the presence of complexes **1-4**. [DNA] = 10 μM, [Complex] = 0−100μM, [EB] = 10 μM. Arrow shows that the emission intensity changes upon increasing complex concentration.

Fig.6 Stern−Volmer (A) and Scatchard (B) plot of the BSA fluorescence titration for complexes **1-4**.

Fig.7 Time dependent effect of ruthenium complexes on reactive oxygen species generation.

Fig.8 PI staining images of DNA damage in A549 cells after treatment with ruthenium complexes (C-control, 1- complex **1**, 2- complex **2**, 3- complex **3** and 4- complex **4)**

Fig. S1 ESI-mass spectrum of complex **1**

Fig. S2 ESI-mass spectrum of complex **2**

Fig. S3 ESI-mass spectrum of complex **3**

Fig. S4 ESI-mass spectrum of complex **4**

Fig. S5 Electronic spectra of complex 3 in Tris-HCl buffer upon the addition of CT-DNA. [Complex] = 25 μM, [DNA] = 0−20 μM. Arrow shows that the absorption intensities decrease upon increasing DNA concentration.

Fig. S6 Electronic spectra of complex 4 in Tris-HCl buffer upon the addition of CT-DNA. [Complex] = 25 μM, [DNA] = 0−20 μM. Arrow shows that the absorption intensities decrease upon increasing DNA concentration.

Fig. S7 Synchronous spectra of BSA (1×10^{-6} M) as a function of concentration of the complex (0-10 μM) with wavelength difference of $\Delta\lambda$= 15 nm), Arrow indicates the change in emission intensity with respect to concentration of complexes 1-4.

Fig. S8 Synchronous spectra of BSA (1×10^{-6} M) as a function of concentration of the complex (0-10 μM) with wavelength difference of $\Delta\lambda$=60 nm), Arrow indicates the change in emission intensity with respect to concentration of complexes **1-4**.

Graphical abstract

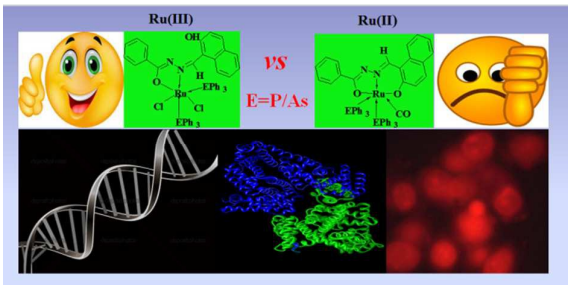

Ruthenium(III) and ruthenium(II) hydrazone complexes were synthesized in one-pot and characterized by spectral and single crystal XRD. Their DNA/BSA binding capability and *in vitro* cytotoxic potential were evaluated.